Superfast quarks in deuterium

Dmitriy N. Kim and Gerald A. Miller
Department of Physics, University of Washington, Seattle, Washington 98195-1560, USA

(Received 26 September 2023; accepted 21 February 2024; published 3 April 2024)

An extension to our previous study on nuclear parton distribution functions (nPDFs) [Kim and Miller, Phys. Rev. C **106**, 055202 (2022)] using light-front holographic quantum chromodynamics (LFHQCD) [Brodsky, de Teramond, Dosch, and Erlich, Phys. Rep. **584**, 1 (2015)] is presented. We apply the effects of nucleon motion inside the nucleus (Fermi motion/smearing) to deuterium, extending our deuterium nPDFs to the *superfast*, $x > 1$, region [Frankfurt and Strikman, Phys. Rep. **160**, 235 (1988)] where we estimate our results to be reasonable up to $x \approx 1.7$. We utilize four different deuteron wave functions (AV18, NijmI, NijmII, Nijm93). We find that our model, with no additional new parameters, shows very good agreement with deuterium EMC ratio data obtained from the BONuS experiment [Fenker *et al.*, Nucl. Instrum. Methods Phys. Res. A **592**, 273 (2008); Baillie *et al.* (CLAS Collaboration), Phys. Rev. Lett. **108**, 142001 (2012); **108**, 199902(E) (2012); Tkachenko *et al.* (CLAS Collaboration), Phys. Rev. C **89**, 045206 (2014); **90**, 059901(E) (2014); Griffioen *et al.*, Phys. Rev. C **92**, 015211 (2015)]. Looking beyond conventional nuclear physics, and in anticipation of 12 GeV experiments at Jefferson Lab, we use a LFHQCD ansatz to predict the contributions of an exotic six-quark state to the deuteron F_2 structure function, F_2^D, in the superfast region. We find that the effects of using other potentials are about the same magnitude as six-quark effects—both have small effects in $x < 1$, but have significant contributions at $x > 1$.

DOI: 10.1103/PhysRevC.109.045203

I. INTRODUCTION

Parton distribution functions are ubiquitous in particle physics because they describe the relationship between quantum chromodynamics' (QCDs) basic degrees of freedom, quarks and gluons (partons), and the physical observable states, hadrons. This makes their nuclear counterparts, nuclear PDFs (nPDFs), indispensable tools towards understanding the emergence of intrinsic nuclear properties from the dynamics of their constituent partons. Although parametrizations of nPDFs exist for several nuclei (e.g., [1–4]), they are not as robust as free proton PDFs [5,6] due to a lack of experimental data over a wide kinematic range (for review, see [7]). However, programs to extract nPDFs have been, and are continued to be, supported with the operation of the CERN Large Hadron Collider, a possible 12 GeV upgrade at Jefferson Lab (JLab), and upcoming Electron-Ion Collider (EIC). It is clear that understanding nPDFs, the interplay between nuclear physics and quantum chromodynamics (QCD), is of great interest and a fundamental goal in nuclear science.

The first experimental observation that nPDFs are different than free nucleon PDFs was by the European Muon Collaboration (EMC) [8,9]. They found the ratio of iron to deuterium structure functions to be less than unity in the region $0.3 < x < 0.7$, dubbed the EMC effect; see, e.g., the review [10]. Since then, studies over several decades have discovered more effects in DIS structure function ratios, those being shadowing ($x < 0.1$) [11–13] and antishadowing ($0.1 < x < 0.3$) [12,14,15]. With definitive explanations yet to be confirmed, there has been much experimental and theoretical effort in understanding these $x < 1$ effects.

However, a domain that has received less attention over the years lies in $x > 1$, dubbed the *superfast* region [11]. This region directly probes the short range structure of the nuclear force, delving into nuclear phenomena at high densities [11]. The superfast region garners interest because it directly probes the junction between nuclear physics and QCD; quarks with $x > 1$ cannot be produced by the QCD dynamics of a single free nucleon, they must be generated due to inter-nucleon interactions. As a result, unlike quarks inside a free nucleon, a quark inside a nucleus can have a momentum fraction as large as $x = A$, where A is the mass number of the nucleus. Therefore, working towards understanding intersections between nuclear physics and QCD must involve investigating superfast quarks.

Nuclear DIS at high-x gives us an opportunity to probe the superfast region. By extracting the DIS F_2 structure function of the nucleus, F_2^A, we can study the $x > 1$ momentum distributions of quarks inside a nucleus. To date, three experiments have undergone such an investigation: The BCDMS Collaboration at CERN [16], the CCFR Collaboration at Fermi Lab [17], and most recently at JLab [18]. However, the trends of F_2^A at high-x, extracted from all three experiments, do

not agree with each other. The experiment at JLab originally reported results in agreement with BCDMS [18]. However, a recent study by Freese *et al.* [19] improved on the Q^2 evolution procedure used in the JLab study, obtaining results slightly in favor of BCDMS, but overall not strongly aligning with either of the two experiments. There is still much experimental work to be done in extracting the behavior of F_2^A in the superfast region. The possible 12 GeV beam energy upgrade at JLab hopes to accomplish this by improving on its predecessors results. The experiment aims to extract F_2^A at an even larger x threshold, in kinematics where quasielastic contributions and scaling violations in the cross section are minimized [20,21].

In contrast to experimental progress, there has been little theoretical work towards F_2^A at $x > 1$ (see review [11] and Ref. [22] for discussion on proposed models). This study focuses on developing a light-front holographic quantum chromodynamics (LFHQCD) model for F_2^D and predict its behavior in the $x > 1$, superfast region. The contents of this paper are as follows. In Sec. II, the light-front (LF) convolution model developed in Refs. [11,23] is introduced, which connects nuclear and bound-nucleon F_2 structure functions. The model achieves this by incorporating the conventional nuclear physics of Fermi motion (nucleon motion inside the nucleus) to bound-nucleon structure functions, outputting F_2^A for $0 < x < A$—our first steps into the superfast region. Following this, we will discuss what will be used as inputs into the convolution model: the LF density matrix of nucleons inside deuterium [11,23], and LFHQCD model for bound-nucleon PDFs [24]. Afterwards, results for the convolution model are presented for different deuteron wave functions (AV18, NijmI, NijmII, Nijm93). In Sec. III, a six-quark LFHQCD ansatz for deuterium is introduced and incorporated into results in Sec. II. Our concluding remarks and discussion are given in Sec. IV.

II. NUCLEAR STRUCTURE FUNCTIONS

The central theoretical objective to be addressed is the nuclear structure function $F_2^A(x, Q^2)$. Within the parton model, $F_2^A(x, Q^2)$ is connected to unpolarized nPDFs of flavor f, $f^A(x, Q^2)$. With the goal of understanding how nuclear dynamics impacts the QCD dynamics of its constituent partons, a theoretical relationship between nPDFs and nucleonic PDFs must be utilized. This can be achieved by expressing nPDFs as a convolution between nucleonic PDFs and a nuclear LF density matrix, incorporating the effects of Fermi motion to nucleonic PDFs (see Refs. [11,23] for discussion and derivation). Furthermore, discovery of the EMC effect (see original work [8]) tells us that the momentum distributions of quarks inside bound nucleons are different than those of free nucleons. Therefore, nucleonic PDFs in the convolution model should be replaced with respective *bound* PDFs. Thus for $F_2^A(x, Q^2)$, in the Bjorken limit (photon virtuality, Q^2, and energy, ν, go to infinity at fixed $x = Q^2/2m\nu$. Note that in this study, we are using isospin symmetry where $m = (m_p + m_n)/2$, introducing negligible errors in our calculations), the convolution formula takes the following form [11,23]:

$$F_2^A(x, Q^2) = \sum_N \int_x^A \frac{d\alpha}{\alpha} \int d^2\boldsymbol{k}_\perp \, \rho_{N/A}(\alpha, \boldsymbol{k}_\perp) \times \tilde{F}_2^N(x/\alpha, \alpha, \boldsymbol{k}_\perp, Q^2), \tag{1}$$

where $\rho_{N/A}(\alpha, \boldsymbol{k}_\perp)$ is the LF density matrix of nucleon N inside nucleus A, $\tilde{F}_2^N(x/\alpha, \alpha, \boldsymbol{k}_\perp, Q^2)$ is the bound nucleon F_2 structure function, $\boldsymbol{k}_\perp$ is the transverse momentum of the nucleon, and $\alpha = A\,k^+/k_A^+$ is the scaled LF momentum fraction carried by nucleon N inside nucleus A. Note that $\tilde{F}_2^N$ is a function of α and $\boldsymbol{k}_\perp$, in addition to x/α and Q^2, due to medium modifications.

In this study, we investigate the F_2 structure function of the deuteron, $F_2^D(x, Q^2)$. To do so, Eq. (1) tells us that we need to determine its LF density matrix, $\rho_{N/D}(\alpha, \boldsymbol{k}_\perp)$, and bound nucleon structure functions, $\tilde{F}_2^N(x/\alpha, \alpha, \boldsymbol{k}_\perp, Q^2)$.

A. Deuteron light-front density matrix

The nuclear LF density matrix for nucleon N inside nucleus A is formally defined in terms of the nuclear LF wave function (LFWF), ψ_A [11,23]:

$$\rho_{N/A}(\alpha, \boldsymbol{k}_\perp) = \int \left[\prod_{i=1}^A \frac{d\alpha_i}{\alpha_i} d^2\boldsymbol{k}_{i\perp}\right] \psi_A^\dagger(\alpha_1, \ldots, \alpha_A, \boldsymbol{k}_{1\perp}, \ldots, \boldsymbol{k}_{A\perp}) \, \psi_A(\alpha_1, \ldots, \alpha_A, \boldsymbol{k}_{1\perp}, \ldots, \boldsymbol{k}_{A\perp}) \times \delta^{(1)}\left(1 - \frac{\sum_{i=1}^A \alpha_i}{A}\right) \delta^{(2)}\left(\sum_{i=1}^A \boldsymbol{k}_{i\perp}\right) \left\{ \sum_{i=1}^{(Z,A-Z)} \alpha_i \, \delta^{(1)}(\alpha - \alpha_i) \, \delta^{(2)}(\boldsymbol{k}_\perp - \boldsymbol{k}_{i\perp}) \right\}, \tag{2}$$

where the upper limit of the sum in the curly brackets is Z for the proton and $A - Z$ for the neutron. The LF density matrix obeys the baryon and momentum sum rules:

$$\sum_N \int_0^A \frac{d\alpha}{\alpha} \int d^2\boldsymbol{k}_\perp \, \rho_{N/A}(\alpha, \boldsymbol{k}_\perp) = A, \tag{3}$$

$$\sum_N \int_0^A \frac{d\alpha}{\alpha} \int d^2\boldsymbol{k}_\perp \, \alpha \, \rho_{N/A}(\alpha, \boldsymbol{k}_\perp) = A. \tag{4}$$

References [11,23], by neglecting all but the nucleonic degrees of freedom and identifying the internal pn configurations in the deuteron through the pn LF momentum,

$$k = \sqrt{\frac{m^2 + k_\perp^2}{\alpha(2-\alpha)} - m^2}, \tag{5}$$

are able to connect the deuteron LFWF, ψ_D, to its nonrelativistic wave function, ψ_{NR}:

$$|\psi_D(k)|^2 = |\psi_{NR}(k)|^2\sqrt{m^2+k^2}. \tag{6}$$

Equation (6) leads to the following expression for the LF density matrix of protons and neutrons in deuterium:

$$\rho_{pn/D}(\alpha, \mathbf{k}_\perp) = \frac{|\psi_{NR}(k)|^2}{2-\alpha}\sqrt{m^2+k^2}, \tag{7}$$

where the subscript *pn* was used as the proton and neutron have identical LF density matrices in the deuteron. One can check that Eq. (7) obeys both sum rules.

B. Bound nucleon F_2 structure function

For the bound nucleon F_2 structure function, we utilize the phenomenological model developed in Ref. [24]. The model employed LFHQCD, a semiclassical approximation to QCD that displays remarkable connections between LF dynamics and gravity in a higher-dimensional anti–de Sitter (AdS) space. It succeeds in reproducing many dynamical and spectroscopic features of QCD, such as Regge trajectories and elastic form factors for mesons and hadrons [25]. The model in Ref. [24], which we will refer as the nuclear LFHQCD (nLFHQCD) model for brevity, outputs closed-form expressions for valence nPDFs that are dependent on two phenomenological parameters, $\delta r_{p/A}$ and $\delta r_{n/A}$. The parameters are proportional to the average virtuality, a quantity that measures the average off-shell-ness of a nucleon inside the nucleus. The nPDFs were used to construct $\tilde{F}_2^N$, given by

$$\begin{aligned}\tilde{F}_2^N\big(x, Q_o^2\big) &= \tfrac{4}{9}\,x\,\tilde{u}^N\big(x, Q_o^2\big) + \tfrac{1}{9}\,x\,\tilde{d}^N\big(x, Q_o^2\big)\\ &= F_2^N\big(x, Q_o^2\big) + \tfrac{5}{3}\,x\,\big(q_4\big(x, Q_o^2\big) - q_3\big(x, Q_o^2\big)\big)\,\delta r_{N/A},\end{aligned} \tag{8}$$

$$\begin{aligned}\tilde{u}^p\big(x, Q_o^2\big) &= \big(\tfrac{3}{2} - 3\delta r_{p/A}\big)q_3\big(x, Q_o^2\big)\\ &\quad + \big(\tfrac{1}{2} + 3\delta r_{p/A}\big)q_4\big(x, Q_o^2\big),\end{aligned} \tag{9}$$

$$\tilde{d}^p\big(x, Q_o^2\big) = (-3\delta r_{p/A})q_3\big(x, Q_o^2\big) + \big(1 + 3\delta r_{p/A}\big)q_4\big(x, Q_o^2\big), \tag{10}$$

where $\tilde{u}^p(x)$ and $\tilde{d}^p(x)$ are the medium-modified proton up and down valence PDFs, respectively, F_2^N is the structure function of free nucleon N, and Q_o is the matching scale between LFHQCD and perturbative QCD, $Q_0 = 1.06 \pm 0.15$ GeV [26]. The neutron valence PDFs are obtained by replacing $\tilde{u}^p \to \tilde{d}^n$, $\tilde{d}^p \to \tilde{u}^n$, and $\delta r_{p/A} \to \delta r_{n/A}$. The function $q_\tau(x, Q_o^2)$ is given by

$$q_\tau\big(x, Q_o^2\big) = \frac{\Gamma(\tau - \frac{1}{2})}{\sqrt{\pi}\,\Gamma(\tau - 1)}(1 - w(x))^{\tau-2}\,w(x)^{-1/2}\,w'(x), \tag{11}$$

$$w(x) = x^{1-x}e^{-a(1-x)^2} \tag{12}$$

with normalization

$$\int_0^1 dx\, q_\tau\big(x, Q_o^2\big) = 1, \tag{13}$$

where the flavor-independent parameter $a = 0.531 \pm 0.037$ and τ is the number of constituents. The modified structure functions were used to construct F_2^A, and numerical results for the phenomenological parameters were obtained by fitting to EMC ratio data in the region $0.3 \leqslant x \leqslant 0.7$ (EMC region). The results of the fitting were successful in reproducing EMC ratio data for a variety of nuclei. Having the correct behavior in the EMC region, the nLFHQCD model is an excellent candidate for $\tilde{F}_2^N$.

In the nLFHQCD model, the virtuality is not kinematical. In other words, nLFHQCD uses the average virtuality of a bound nucleon inside a nucleus, characterized by a single, nucleus-dependent number, and does not depend on detailed values of nucleon kinematics. This is because the model treats the nuclear potential as a constant. To improve on this we will use an ansatz motivated by results in Ref. [24], where $\delta r_{p/A}(\alpha, \boldsymbol{k}_\perp)$ and $\delta r_{n/A}(\alpha, \boldsymbol{k}_\perp)$ are proportional to virtuality which depends on nucleon kinematics, up to a constant

$$\delta r_{N/A}(\alpha, \boldsymbol{k}_\perp) = -\eta\,\mathcal{V}_{N/A}(\alpha, \boldsymbol{k}_\perp)\,\theta(1-\alpha). \tag{14}$$

Here, $\mathcal{V}_{N/A}(\alpha, \boldsymbol{k}_\perp)$ is the virtuality of bound nucleon N inside nucleus A, η is a nucleus-independent fitting parameter, and $\theta(1-\alpha)$ is the Heaviside step function. The nLFHQCD model was constructed to incorporate off-shell effects for single nucleons that are limited to carry $\alpha < 1$ momentum fraction. Therefore, extending off-shell effects beyond $\alpha > 1$ would exceeding the model's limits of applicability, hence the Heaviside step function in Eq. (14).

For the deuteron, in the center of mass frame, we use the following definition for virtuality:

$$\begin{aligned}\mathcal{V}_{pn/D}(\alpha, \boldsymbol{k}_\perp) &\equiv \frac{k_D^- - (k_p^- + k_n^-)}{k_D^-}\\ &= \frac{1}{m_D^2}\left(m_D^2 - 4\frac{m^2 + k_\perp^2}{\alpha(2-\alpha)}\right),\end{aligned} \tag{15}$$

instead of $\mathcal{V} \equiv (k^2 - m^2)/m^2$, as used in Ref. [24]. This is because the convolution formula in Eq. (1) was obtained by using LF perturbation theory, where intermediate states are on mass shell, $k^2 = m^2$, but off their energy shells, $k_D^- \neq k_p^- + k_n^-$. Equation (15) is constructed to be negative, which is required to obtain the correct modification for the EMC region. The connection between 'LF' virtuality, Eq. (15), and equal-time (ET) virtuality, $\mathcal{V} \equiv (k^2 - m^2)/m^2$, within the BLC-PLC model used in Ref. [24] is discussed in Appendix A.

For completeness, we would like to mention the work of Ref. [27], which uses the soft-wall AdS/QCD model to study the elastic form factors and structure functions of deuterium—another example of using AdS/QCD models to study nuclei. They accomplished this by working with an effective action that comprised of vector fields dual to the deuteron. From this effective action they were able to obtain expressions for the form factors and achieved very good fits to experimental data.

III. LIGHT-FRONT CONVOLUTION MODEL RESULTS

First, we would like to stress that all the structure function results in this study become less reliable for $x >\approx 1.7$. Probing larger values of x requires knowledge of the nucleon

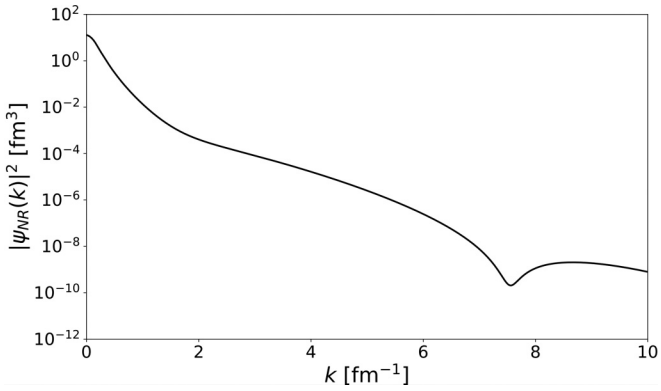

FIG. 1. A plot of the interpolated AV18 nucleon momentum distribution in deuterium in the region $0 < k < 10$ fm^{-1}.

momentum distribution at high momenta, where nucleons begin to overlap significantly. Here, QCD effects will begin to contribute to the dynamics, and the picture of nucleonic degrees of freedom begin to break down. As a result, the approximation used to obtain Eq. (6) becomes invalid at momenta needed to probe $x > \approx 1.7$. The estimate was obtained by using Eq. (5) and setting $k_\perp = 0$, assuming that nucleonic degrees of freedom begin to break down when the nucleon momenta reach around the mass of the proton, ≈1000 MeV. However, by imposing the inclusive quark counting rule for F_2^D in Ref. [28], under the assumption that F_2^D has no off-shell effects at $x > 1$, one can determine the asymptotic $\alpha \to 2$ behavior of the deuteron LFWF in the convolution model. More discussion can be found in Appendix B.

For the nucleon momentum distribution in deuterium, $|\psi_{NR}(k)|^2$, we used the AV18 wave function [29], unless stated otherwise, and the following normalization was used:

$$\int_0^\infty |\psi_{NR}(k)|^2 4\pi k^2 dk = 1. \tag{16}$$

The momentum distribution was tabulated for finite points of k, the magnitude of the total momentum, and an interpolator was used. Figure 1 presents the nucleon momentum distribution in deuterium for a k range of $0 < k < 10$ fm^{-1}. The tabulated data was in the range $0 < k < 20$ fm^{-1}, anything outside this range was evaluated to be 0.

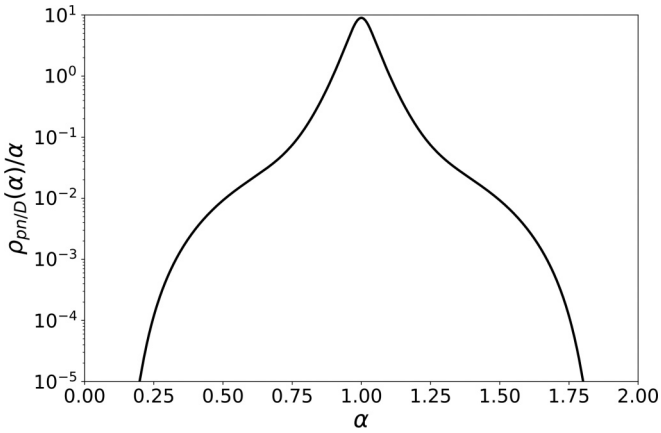

FIG. 2. The proton and neutron LF density matrices for deuterium, divided by α, as a function of α, the momentum fraction of the nucleon in the nucleus weighted by A.

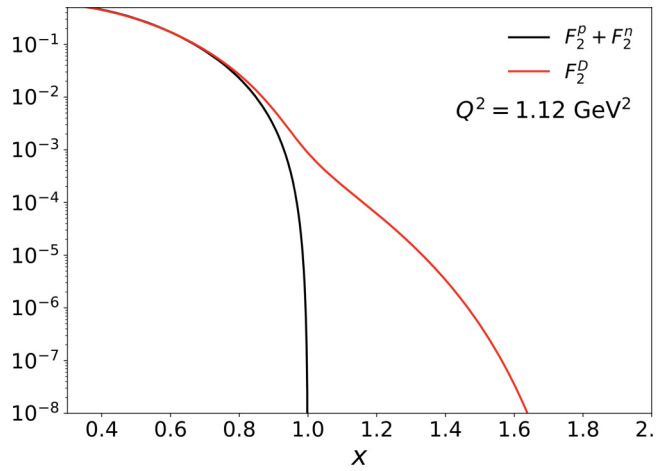

FIG. 3. DIS F_2 structure functions on a logarithmic y-axis, evaluated at $Q^2 = 1.12$ GeV^2. The solid black line is the sum of the free proton and neutron structure functions and the solid red line was obtained by using Eq. (1).

Using the AV18 momentum distribution, we obtained the LF density matrix by using Eq. (7). The LF density matrix for nucleons in deuterium, divided by α, is presented in Fig. 2.

Finally, using Eq. (1) we obtained F_2^D, evaluated at $Q^2 = 1.12$ GeV^2. The results are presented in Fig. 3. The value used for the constant η in Eq. (14) was taken to be 0.4 ± 0.1, motivated by results in the nLFHQCD model [24]. Discussion on η in the blob-like component - point-like component (BLC-PLC) model can be found in Appendix A.

Figure 4 presents results for F_2^D, Eq. (1), using the Nijmegen (NijmI, NijmII, Nijm93) [30,31] and AV18 wave functions [29], displaying the model's sensitivity to different

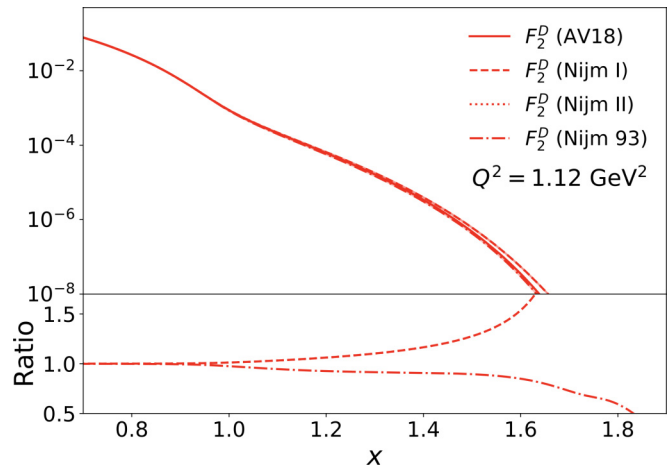

FIG. 4. (Top) Results for F_2^D, Eq. (1), using different deuteron wave functions. The sold red line uses the AV18 wave function and the dashed, dotted, and dot-dashed red lines use the NijmI, NijmII, and Nijm93 wave functions, respectively. (Bottom) The ratios of the Nijm F_2^D results with respect to the AV18 results. Note that NijmI and NijmII lines are overlapped.

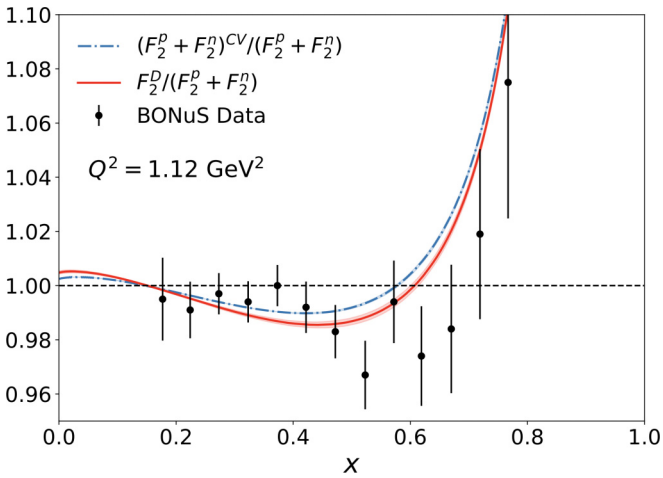

FIG. 5. All DIS F_2 quantities are evaluated at $Q^2 = 1.12$ GeV^2. The solid red line is the convolution model nLFHQCD result using Eq. (1), the dot-dashed blue line was obtained by using free nucleon structure functions in Eq. (1), where the superscript *CV* means 'convolution', and the filled black points are experimental results obtained from the BONuS experiment [32–35].

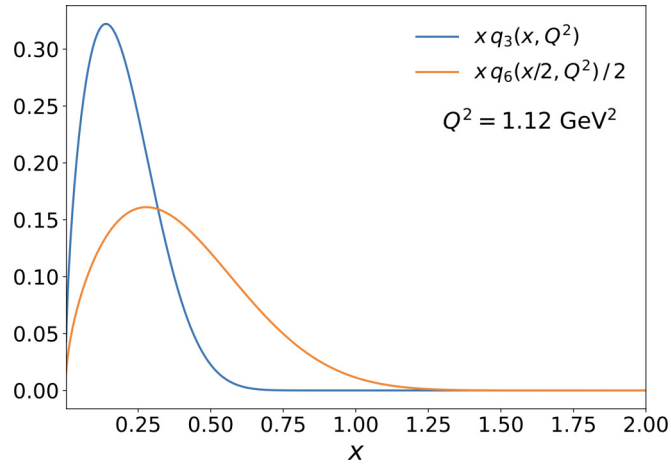

FIG. 6. Comparison between $xq_3(x, Q^2)$ distribution used in bound-nucleon PDFs in Eqs. (9), (10), and the six-quark PDF ansatz used in Eq. (19), $xq_6(x/2, Q^2)/2$, evaluated at $Q^2 = 1.12$ GeV^2.

nucleon-nucleon potentials. All deuteron wave functions were normalized according to Eq. (16). We find that results using different nucleon-nucleon potentials agree in the $x < 1$ region, and begin to diverge when $x > 1$, with differences as large at 50%.

Figure 5 presents the results for the EMC ratio for deuterium. All DIS F_2 quantities are evaluated at $Q^2 = 1.12$ GeV^2. Our results for $F_2^D/(F_2^p + F_2^n)$ give a $\chi^2 = 1.03$, in very good agreement with data obtained from the BONuS experiment, which extracted F_2^n/F_2^D by using a spectator tagging technique on semi-inclusive electron-deuteron collisions [32–35]. Notice that simply applying Fermi smearing to $F_2^p + F_2^n$ yields a deuterium EMC effect that captures data as well with a $\chi^2 = 1.18$.

IV. ADDITION OF SIX-QUARK CLUSTER

With the LF convolution model F_2^D result, we can now explore ideas outside conventional nuclear physics by including QCD effects in the superfast region. Motivated towards understanding intersections between nuclear physics and QCD, we model the PDFs for an exotic six-quark state to make predictions on its contribution to F_2^D (see Ref. [36] for discussion on hidden color states and the behavior of form factors at large Q^2 in deuterium). Deuterium can occupy a six-quark state through quantum fluctuations, causing the proton and neutron to overlap completely. This six-quark cluster/bag, compared to a bound proton and neutron, allows for a greater sharing of momentum between the quarks in deuterium, enhancing the distribution of high-momentum quarks [20]. However, since most of deuteron's properties can be described by the picture of a bound proton and neutron with pionic effects, we expect the six-quark bag probability, P_{6q}, to be very small. A previous study investigated the contribution of a six-quark state to the b_1 structure function of the deuteron [37]. The study used a six-quark probability of $P_{6q} = 0.15\%$ to match the experimental extraction of b_1 at $x = 0.452$ by the HERMES Collaboration [38]. Since this value for the probability was obtained from fitting to one point, we will use it as a conservative upper bound for P_{6q}.

Now we need to model the PDF of a six-quark hadronic state in order to get its DIS F_2 structure function,

$$F_2^{6q}(x, Q^2) = \frac{4}{9}\frac{x}{2}\,u^{6q}(x/2, Q^2) + \frac{1}{9}\frac{x}{2}\,d^{6q}(x/2, Q^2), \quad (17)$$

where $u^{6q}(x/2, Q^2)$ and $d^{6q}(x/2, Q^2)$ are the up and down PDFs of the six-quark state. To include the contributions of a six-quark cluster to F_2^D, we added Eq. (17) to Eq. (1), multiplying both terms by a six-quark probability factor—not applying the convolution model to Eq. (17) as a six-quark cluster does not have moving-nucleonic components:

$$F_2^D(x, Q^2) = (1.0 - P_{6q}) \sum_N \int_x^A \frac{d\alpha}{\alpha} \int d\boldsymbol{k}_\perp\, \rho_{N/D}(\alpha, \boldsymbol{k}_\perp) \times \tilde{F}_2^N(x/\alpha, \alpha, \boldsymbol{k}_\perp, Q^2) + P_{6q} F_2^{6q}(x, Q^2). \quad (18)$$

Now, the theoretical issue is to determine an ansatz for the PDFs of a six-quark state in deuterium.

A. LFHQCD six-quark ansatz

We use the LFHQCD formalism to describe the quark PDFs of a six-quark cluster as

$$u^{6q}\big(x/2, Q_o^2\big) = d^{6q}\big(x/2, Q_o^2\big) = \tfrac{3}{2}\, q_6\big(x/2, Q_o^2\big). \quad (19)$$

The six-quark PDFs use the same q_τ as in Eq. (11), which incorporates Regge behavior at small x, and inclusive counting rules at $x \to 1$. Furthermore, we focus on the contributions of the valence quarks and do not include the contributions of higher Fock states in Eq. (19). Figure 6 shows a comparison between $xq_3(x, Q^2)$, used in the bound-nucleon PDFs, and the exotic six-quark PDF ansatz, $xq_6(x/2, Q^2)/2$.

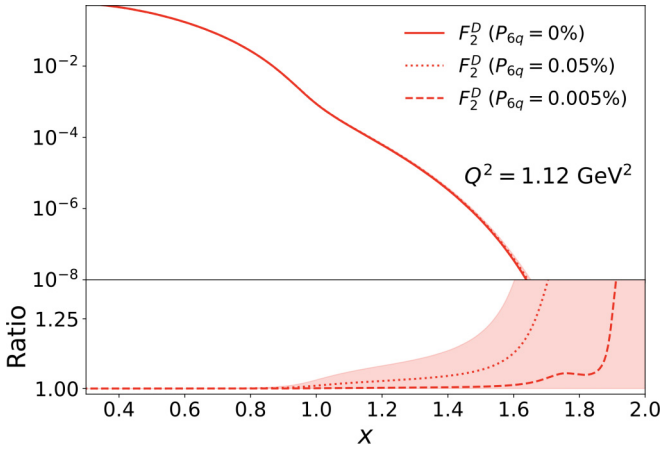

FIG. 7. (Top) DIS F_2 structure functions on a logarithmic y axis. All F_2 quantities are evaluated at $Q^2 = 1.12$ GeV^2. (Bottom) The ratios $F_2^D(P_{6q})/F_2^D(P_{6q} = 0\%)$. The predicted six-quark contribution is displayed as a filled-in red volume, but is difficult to discern on the top plot with the given axis scaling. The lower boundary of the volume is $P_{6q} = 0\%$ and the upper boundary is $P_{6q} = 0.15\%$. The red dotted and dashed lines display $P_{6q} = 0.05\%$ and $P_{6q} = 0.005\%$, respectively, and are shown to clarify the trend of F_2^D with varying F_2^{6q} contributions.

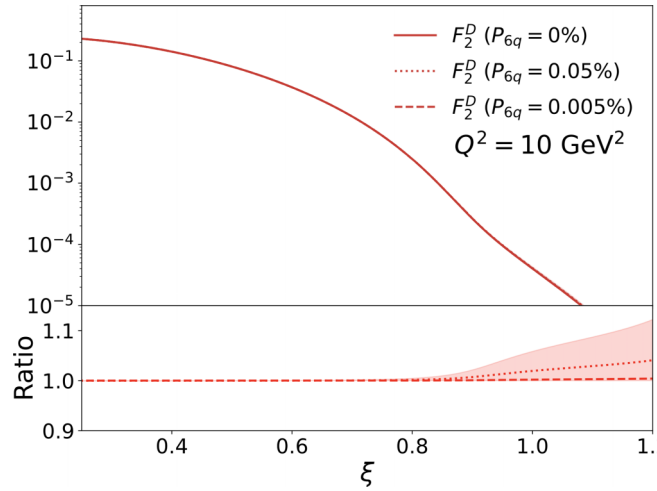

FIG. 8. (Top) DIS F_2 structure functions on a logarithmic y-axis, as a function of the Nachtmann variable, ξ, evaluated at $Q^2 = 10$ GeV^2. (Bottom) The ratios $F_2^D(P_{6q})/F_2^D(P_{6q} = 0\%)$. The predicted six-quark contribution is displayed as a filled-in red volume, but is difficult to discern on the top plot with the given axis scaling. The lower boundary of the volume is $P_{6q} = 0\%$ and the upper boundary is $P_{6q} = 0.15\%$. The red dotted and dashed lines display $P_{6q} = 0.05\%$ and $P_{6q} = 0.005\%$, respectively, and are shown to clarify the trend of F_2^D with varying F_2^{6q} contributions.

By combining Eqs. (17), (19) we obtained

$$F_2^{6q}(x, Q_o^2) = \frac{5}{9}\frac{x}{2}\left(\frac{3}{2}\, q_6\big(x/2, Q_o^2\big)\right). \tag{20}$$

Notice that the argument of q_6 is $x/2$, this ensures that the up and down six-quark PDFs extend to $x = 2$. Figure 7 presents the predictions of the LFHQCD six-quark model to our convolution model results from Sec. II, evaluated at $Q^2 = 1.12$ GeV^2. Notice that six-quark contributions dominate at $x > 1$.

Figure 8 presents the same information as Fig. 17, but as a function of the Nachtmann variable, $\xi = 2x/(1 + \sqrt{1 + 4m^2x^2/Q^2})$, a common prescription for target mass corrections and displays scaling even at large values of ξ (for more discussion see Refs. [18,20,39]). The results are evaluated at $Q^2 = 10$ GeV^2, kinematics that are within the proposed reach of 12 GeV JLab experiments [20,21]. To accomplish this, the PDFs are evolved to a higher scale with the Dokshitzer-Gribov-Lipatov-Altarelli-Parisi (DGLAP) equations [40–42] using the APFEL package [43]. The inputs for DGLAP evolution, such as the initial scale, renormalization scheme, and heavy quark thresholds, are identical to the ones used to study PDFs in LFHQCD in Ref. [26].

V. DISCUSSION AND CONCLUSION

The results presented in this paper are an extension to our previous study in Ref. [24]. Focusing on the deuteron, we applied Fermi motion effects using a variety of different wave functions to extend the nLFHQCD model beyond $x > 1$ with reasonable model predictions up to $x \approx 1.7$. In doing so, we found that our model is in very good agreement to BONuS data for the EMC ratio [32–35], and that the effects of different nucleon-nucleon potentials become significant in the superfast region. On top of conventional nuclear physics, we implemented the contributions of an exotic six-quark state to F_2^D using a LFHQCD ansatz [27]. We found that the six-quark distribution enhances the $x > 1$ region, while minimally affecting $x < 1$—displaying correct qualitative behavior as a six-quark cluster allows for a greater sharing of momentum between quarks, enhancing the high-momentum behavior of F_2^D, while minimally affecting the low-momentum region. We displayed the predictions of the six-quark ansatz to F_2^D for $0 < P_{6q} < 0.15\%$ in Fig. 7, with the upper bound in P_{6q} motivated by Ref. [37]. We found that a small six-quark probability, $P_{6q} = 0.15\%$ can lead to large enhancements in the superfast region, enhancements greater than 25% for $x > 1.6$. Furthermore, we found that the effects of different nucleon-nucleon potentials are around the same magnitude as six-quark effects in our model. With the proposed 12 GeV experiments at JLab, we hope to test these predictions against experimental data in the near future. Deviations from the following predictions could be an indication of more interesting physics in the superfast region.

ACKNOWLEDGMENTS

D.N.K. and G.A.M. would like to thank John Arrington for motivating this study and Adam Freese, Mark Strikman, Stanley J. Brodsky, and Guy F. de Teramond for fruitful discussions. This work was supported by the U.S. Department of Energy Office of Science, Office of Nuclear Physics under Award No. DE-FG02-97ER41014.

APPENDIX A: RELATIONSHIP BETWEEN LIGHT-FRONT AND EQUAL-TIME VIRTUALITY IN BLC-PLC MODEL

First, we need to determine the connection between Eq. (15) and the nucleon-nucleon potential. Using LF perturbation theory one can obtain the Weinberg equation, which in the vicinity of the deuteron bound state, becomes the following Schrodinger-like equation for the wave function of the deuteron without spin and isospin effects [23,44]:

$$\left(M_{1,2}^2 - M_D^2\right)\psi_D(\alpha,\boldsymbol{k}_\perp) = \Gamma(\alpha,\boldsymbol{k}_\perp) = \int V(\alpha',\boldsymbol{k}'_\perp,\alpha,\boldsymbol{k}_\perp)\psi_D(\alpha',\boldsymbol{k}'_\perp) \times \frac{d\alpha'}{\alpha'(2-\alpha')}\frac{d^2\boldsymbol{k}'_\perp}{(2\pi)^3}, \tag{A1}$$

$$M_{1,2}^2 = 4\,\frac{m^2+\boldsymbol{k}_\perp^2}{\alpha(2-\alpha)}. \tag{A2}$$

Here, $M_{1,2}^2$ is the invariant mass of the two nucleon system, M_D^2 is the squared mass of the deuteron, $V(\alpha',\boldsymbol{k}'_\perp,\alpha,\boldsymbol{k}_\perp)$ is the nucleon-nucleon potential, and $\psi_D(\alpha,\boldsymbol{k}_\perp)$ is the LF deuteron wave function. The symbol $\Gamma(\alpha,\boldsymbol{k}_\perp)$ is also known as the bound state vertex function. Neglecting all but nucleonic degrees of freedom and identifying the *pn* components of the deuteron wave function, we can use Eq. (5) to relate the LF deuteron wave equation to the conventional nonrelativistic Schrodinger equation for deuterium:

$$4\left(k^2+k_D^2\right)\psi_D(k) = \Gamma(k) = \int V(k,k')\,\psi_D(k')\,\frac{d^3\boldsymbol{k}'}{(2\pi)^3\sqrt{m^2+k'^2}}, \tag{A3}$$

where $k_D^2 = m^2 - (M_D^2/4)$. Using Eq. (15), we can express the left-hand side of Eq. (A3) as

$$4\left(k^2+k_D^2\right)\psi_D(k) = -M_D^2\,\mathcal{V}_{pn/D}(k)\,\psi_D(k). \tag{A4}$$

With Eqs. (A3), (A4), we get

$$\mathcal{V}_{pn/D}(\alpha,\boldsymbol{k}_\perp) = -\frac{1}{M_D^2}\frac{\Gamma(k)}{\psi_D(k)}, \tag{A5}$$

displaying the relationship between LF virtuality for the deuteron, the deuteron wave function, and the nucleon-nucleon potential.

Now we want to apply the BLC-PLC model used in Ref. [24] to Eq. (A5). Note that the BLC-PLC model neglects spin and isospin effects, and treats the nuclear potential with a number, thus Eq. (A5) is applicable. The simplified nucleon-nucleon potential in momentum space must take the following form to match the potential used in the BLC-PLC model:

$$V(k,k') = (2m)^2\,|U_{NN}|\,(2\pi)^3\,\delta^{(3)}(\boldsymbol{k}-\boldsymbol{k}'), \tag{A6}$$

where $|U_{NN}|$ is the simplified nucleon-nucleon potential used for deuteron in the BLC-PLC model, and the $(2m)^2$ factor is the relativistic normalization factor which connects relativistic and nonrelativistic scattering matrix elements. Plugging in Eq. (A6) into Eq. (A5) we obtain

$$\mathcal{V}_{pn/D}(\alpha,\boldsymbol{k}_\perp) = -\frac{(2m)^2}{M_D^2}\frac{|U_{NN}|}{\sqrt{m^2+k^2}}, \tag{A7}$$

which in the nonrelativistic limit, and taking $2m \approx M_D$, becomes

$$\mathcal{V}_{pn/D}(\alpha,\boldsymbol{k}_\perp) \approx -\frac{|U_{NN}|}{m}. \tag{A8}$$

Reference [24] uses $\mathcal{V} = (m^2+k^2)/m^2$ and obtained the following expression for virtuality:

$$\mathcal{V} = -\frac{2\,|U|}{m}. \tag{A9}$$

Thus we find that LF virtuality is exactly half the ET virtuality in the BLC-PLC model. Defining the average virtuality as

$$\langle\mathcal{V}_{np/D}\rangle = \int_0^A \frac{d\alpha}{\alpha}\int d^2\boldsymbol{k}_\perp \mathcal{V}_{np/D}(\alpha,\boldsymbol{k}_\perp)\,\rho_{np/D}(\alpha,\boldsymbol{k}_\perp), \tag{A10}$$

we obtain $\langle\mathcal{V}_{np/D}\rangle = -0.0235$, which corresponds to a value of -0.047 if using ET virtuality. This is in agreement with the average ET virtuality obtained in Ref. [45]. With Eq. (A8) we determine, using results in Ref. [24],

$$\delta r_{pn/D}(\alpha,\boldsymbol{k}_\perp) = -\frac{m}{4}\frac{\mathcal{V}_{np/D}(k)}{\bar{\Delta}}. \tag{A11}$$

Relating Eq. (A11) with Eq. (14), we find that the constant $\eta = m/(4\bar{\Delta})$. In our study, we used $\eta = 0.4 \pm 0.1$ which gives $\bar{\Delta} \approx 587 \pm 147$ GeV, in agreement with the BLC-PLC model which limits $\bar{\Delta}$ to be greater than or equal to the difference between the Roper resonance and nucleon mass.

APPENDIX B: ASYMPTOTIC $\alpha \to 2$ BEHAVIOR OF THE DEUTERON LF WAVE FUNCTION USING THE CONVOLUTION MODEL

Due to approximations used to obtain Eq. (6) breaking down at large momenta, it is not possible to conclusively predict the asymptotic $x \to 2$ behavior of F_2^D in the convolution model. However, we can make progress in the converse situation and understand the asymptotic behavior of the deuteron LFWF model by imposing quark counting rule constraints [28] to F_2^D. Starting from Eq. (1) and assuming no off-shell modifications to F_2^D at $x > 1$, we expand $\rho(\alpha,\mathbf{k}_\perp)$ and $F_2^N(x/\alpha)$ around $\alpha = 2$, as taking the limit $x \to 2$ causes $\alpha \to 2$ as well:

$$\lim_{x\to2} F_2^D(x,Q^2) \approx \lim_{x\to2}\sum_N \int_x^A \frac{d\alpha}{2}\int d^2\boldsymbol{k}_\perp \times\left[\rho_{N/D}(2,\boldsymbol{k}_\perp) + \rho'_{N/D}(2,\boldsymbol{k}_\perp)(\alpha-2)+\ldots\right] \times\left[F_2^N(x/2) - \frac{x}{4}F_2^{N'}(x/2)(\alpha-2)+\ldots\right]. \tag{B1}$$

In the limit as $x \to 2$, we use the inclusive quark counting rule of Ref. [28], which is obeyed in LFHQCD, to replace F_2^N with $(1-\frac{x}{2})^3$. Performing the α integration one can find that $\rho_{N/D}(2, \boldsymbol{k}_\perp)$ terms go as $(1-\frac{x}{2})^4$, $\rho'_{N/D}(2, \boldsymbol{k}_\perp)$ terms as $(1-\frac{x}{2})^5$, and so on. Therefore, if you restrict F_2^D to obey inclusive quark counting rules, $F_2^D \sim (1-\frac{x}{2})^9$, it must be that the dominant α dependence of $\rho_{N/D}$ in the limit of $\alpha \to 2$ goes like

$$\lim_{\alpha \to 2} \rho_{N/D}(\alpha, \boldsymbol{k}_\perp) \sim (\alpha - 2)^5. \tag{B2}$$

The relationship between the LF density matrix and LFWF for the deuteron is

$$\rho_{N/D}(\alpha, \boldsymbol{k}_\perp) = \frac{|\psi_D(\alpha, \boldsymbol{k}_\perp)|^2}{2-\alpha}. \tag{B3}$$

Thus with the constraint that F_2^D obeys inclusive counting rules the convolution model predicts that the α dependence, in the limit of $\alpha \to 2$, of the deuteron LFWF is as

$$|\psi_D(\alpha, \boldsymbol{k}_\perp)| \sim (\alpha - 2)^3. \tag{B4}$$

[1] K. J. Eskola, P. Paakkinen, H. Paukkunen, and C. A. Salgado, EPPS16: Nuclear parton distributions with LHC data, Eur. Phys. J. C **77**, 163 (2017).

[2] K. Kovařík *et al.*, nCTEQ15 - Global analysis of nuclear parton distributions with uncertainties in the CTEQ framework, Phys. Rev. D **93**, 085037 (2016).

[3] R. Abdul Khalek, J. J. Ethier, and J. Rojo (NNPDF Collaboration), Nuclear parton distributions from lepton-nucleus scattering and the impact of an electron-ion collider, Eur. Phys. J. C **79**, 471 (2019).

[4] M. Walt, I. Helenius, and W. Vogelsang, Open-source QCD analysis of nuclear parton distribution functions at NLO and NNLO, Phys. Rev. D **100**, 096015 (2019).

[5] R. D. Ball *et al.* (NNPDF Collaboration), Parton distributions from high-precision collider data, Eur. Phys. J. C **77**, 663 (2017).

[6] S. Dulat, T.-J. Hou, J. Gao, M. Guzzi, J. Huston, P. Nadolsky, J. Pumplin, C. Schmidt, D. Stump, and C. P. Yuan, New parton distribution functions from a global analysis of quantum chromodynamics, Phys. Rev. D **93**, 033006 (2016).

[7] M. Klasen and H. Paukkunen, Nuclear PDFs after the first Ddecade of LHC data, arXiv:2311.00450 [hep-ph].

[8] J. J. Aubert *et al.* (European Muon Collaboration), The ratio of the nucleon structure functions $F2_n$ for iron and deuterium, Phys. Lett. B **123**, 275 (1983).

[9] J. Gomez *et al.*, Measurement of the A-dependence of deep inelastic electron scattering, Phys. Rev. D **49**, 4348 (1994).

[10] O. Hen, G. A. Miller, E. Piasetzky, and L. B. Weinstein, Nucleon-nucleon correlations, short-lived excitations, and the quarks within, Rev. Mod. Phys. **89**, 045002 (2017).

[11] L. L. Frankfurt and M. I. Strikman, Hard nuclear processes and microscopic nuclear structure, Phys. Rep. **160**, 235 (1988).

[12] M. Arneodo *et al.* (European Muon Collaboration), Shadowing in deep inelastic muon scattering from nuclear targets, Phys. Lett. B **211**, 493 (1988).

[13] L. Frankfurt, V. Guzey, and M. Strikman, Leading twist nuclear shadowing phenomena in hard processes with nuclei, Phys. Rep. **512**, 255 (2012).

[14] L. L. Frankfurt, M. I. Strikman, and S. Liuti, Evidence for enhancement of gluon and valence quark distributions in nuclei from hard lepton nucleus processes, Phys. Rev. Lett. **65**, 1725 (1990).

[15] S. J. Brodsky and H. J. Lu, Shadowing and antishadowing of nuclear structure functions, Phys. Rev. Lett. **64**, 1342 (1990).

[16] A. C. Benvenuti *et al.* (BCDMS Collaboration), Nuclear structure function in carbon near x = 1, Z. Phys. C **63**, 29 (1994).

[17] M. Vakili *et al.* (CCFR Collaboration), Nuclear structure functions in the large-x large-Q^2 kinematic region in neutrino deep inelastic scattering, Phys. Rev. D **61**, 052003 (2000).

[18] N. Fomin *et al.*, Scaling of the F_2 structure function in nuclei and quark distributions at $x > 1$, Phys. Rev. Lett. **105**, 212502 (2010).

[19] A. J. Freese, W. Cosyn, and M. M. Sargsian, QCD evolution of superfast quarks, Phys. Rev. D **99**, 114019 (2019).

[20] J. Arrington *et al.*, Inclusive scattering from nuclei at $x > 1$ in the quasielastic and deeply inelastic regimes, JLab:PR12-06-105, 2006, https://www.jlab.org/exp_prog/proposals/06/PR12-06-105.pdf.

[21] O. Hen, L. B. Weinstein, S. Gilad, and S. A. Wood, In medium nucleon structure functions, SRC, and the EMC effect, arXiv:1409.1717 [nucl-ex].

[22] M. M. Sargsian, Superfast quarks in the nuclear medium, Nucl. Phys. A **782**, 199 (2007).

[23] L. L. Frankfurt and M. I. Strikman, High-energy phenomena, short range nuclear structure and QCD, Phys. Rep. **76**, 215 (1981).

[24] D. N. Kim and G. A. Miller, Light-front holography model of the EMC effect, Phys. Rev. C **106**, 055202 (2022).

[25] S. J. Brodsky, G. F. de Teramond, H. G. Dosch, and J. Erlich, Light-front holographic QCD and emerging confinement, Phys. Rep. **584**, 1 (2015).

[26] G. F. de Teramond, T. Liu, R. S. Sufian, H. G. Dosch, S. J. Brodsky, and A. Deur (HLFHS Collaboration), Universality of generalized parton distributions in light-front holographic QCD, Phys. Rev. Lett. **120**, 182001 (2018).

[27] T. Gutsche, V. E. Lyubovitskij, and I. Schmidt, Deuteron electromagnetic structure functions and polarization properties in soft-wall AdS/QCD, Phys. Rev. D **94**, 116006 (2016).

[28] S. J. Brodsky and G. P. Lepage, Exclusive processes and the exclusive inclusive connection in quantum chromodynamics, SLAC-PUB-2294, Workshop on the Unified Theories and the Baryon Number in the Universe Tsukuba, Japan, February 13-14, 1979.

[29] R. B. Wiringa, R. Schiavilla, S. C. Pieper, and J. Carlson, Nucleon and nucleon-pair momentum distributions in $A \leqslant 12$ nuclei, Phys. Rev. C **89**, 024305 (2014).

[30] V. G. J. Stoks, R. A. M. Klomp, C. P. F. Terheggen, and J. J. de Swart, Construction of high quality N N potential models, Phys. Rev. C **49**, 2950 (1994).

[31] J. J. de Swart, R. A. M. Klomp, M. C. M. Rentmeester, and T. A. Rijken, Few-Body Syst. Suppl. **8**, 438 (1996).

[32] H. C. Fenker *et al.*, BoNuS: Development and use of a radial TPC using cylindrical GEMs, Nucl. Instrum. Methods Phys. Res. A **592**, 273 (2008).

[33] N. Baillie *et al.* (CLAS Collaboration), Measurement of the neutron F2 structure function via spectator tagging with CLAS, Phys. Rev. Lett. **108**, 142001 (2012); **108**, 199902(E) (2012).

[34] S. Tkachenko *et al.* (CLAS Collaboration), Measurement of the structure function of the nearly free neutron using spectator tagging in inelastic ^{2}H(e, e'p)X scattering with CLAS, Phys. Rev. C **89**, 045206 (2014); **90**, 059901(E) (2014).

[35] K. A. Griffioen *et al.*, Measurement of the EMC effect in the deuteron, Phys. Rev. C **92**, 015211 (2015).

[36] S. J. Brodsky, C.-R. Ji, and G. P. Lepage, Quantum chromodynamic predictions for the deuteron form-factor, Phys. Rev. Lett. **51**, 83 (1983).

[37] G. A. Miller, Pionic and hidden-color, six-quark contributions to the deuteron b1 structure function, Phys. Rev. C **89**, 045203 (2014).

[38] A. Airapetian *et al.* (HERMES Collaboration), First measurement of the tensor structure function b(1) of the deuteron, Phys. Rev. Lett. **95**, 242001 (2005).

[39] O. Nachtmann, Positivity constraints for anomalous dimensions, Nucl. Phys. B **63**, 237 (1973).

[40] G. Altarelli and G. Parisi, Asymptotic freedom in parton language, Nucl. Phys. B **126**, 298 (1977).

[41] Y. L. Dokshitzer, Calculation of the structure functions for deep inelastic scattering and e+ e- annihilation by perturbation theory in quantum chromodynamics, Zh. Eksp. Teor. Fiz. **73**, 1216 (1977) [Sov. Phys. JETP **46**, 641 (1977)].

[42] V. N. Gribov and L. N. Lipatov, Deep inelastic electron scattering in perturbation theory, Phys. Lett. B **37**, 78 (1971).

[43] V. Bertone, S. Carrazza, and J. Rojo (APFEL Collaboration), APFEL: A PDF evolution library with QED corrections, Comput. Phys. Commun. **185**, 1647 (2014).

[44] S. Weinberg, Dynamics at infinite momentum, Phys. Rev. **150**, 1313 (1966).

[45] X. G. Wang, A. W. Thomas, and W. Melnitchouk, Do short-range correlations cause the nuclear EMC effect in the deuteron? Phys. Rev. Lett. **125**, 262002 (2020).